Fermi National Accelerator Laboratory

FERMILAB-Conf-94/031

Hyperon Polarization, Crystal Channeling and E781 at Fermilab

Joseph Lach

Fermi National Accelerator Laboratory
P.O. Box 500, Batavia, Illinois 60510

January 1994

Invited talk *U.S./Japan Seminar: The Hyperon-Nucleon Interaction*, Maui, Hawaii, October 25-28, 1993

Disclaimer

Hyperon Polarization, Crystal Channeling, and E781 At Fermilab

Joseph Lach
Fermilab

Abstract

Early experiments at Fermilab observed significant polarization of inclusively produced hyperons. These and subsequent experiments showed that Λ^0 were produced polarized while $\overline{\Lambda}^0$ had no polarization in the same kinematical region. Other hyperons and antihyperons were also seen to be polarized. Recent Fermilab experiments have showed this to be a rich and complex phenomena. Theoretical understanding is still lacking. Fermilab E761 has shown that bent single crystals can be used to precess the polarization of hyperons and from the precession angle measure the hyperon's magnetic moment. This opens the possibility of measuring the magnetic moments of charmed baryons. Finally, I will briefly discuss Fermilab E781, an experiment designed to study charmed particle production by Σ^- hyperons.

High energy hyperon beams with easily controlled polarizations have allowed precision measurements of hyperon static properties. They have allowed us to study polarization effects in Σ^- beta decay [1], high statistics weak radiative decays [2], and to make precision measurements of hyperon magnetic moments [3]. These experiments could be done without a knowledge of the mechanism that produced the polarized hyperons. **You didn't have to understand the polarization process to use it.**

In recent years it has become clear that hyperon polarization itself is a complex process whose energy and p_t dependence is different for each of the hyperons. This has provided significant challenges to our theoretical understanding of polarization mechanisms. Let me familiarize you with some of the basic properties of hyperon beams and the techniques used to study their polarization.

There are a number of reviews describing hyperon beams and the physics programs that have utilized them [4-7].

What are the essential elements of a hyperon beam?

*Start with a high energy proton beam
*Interact the beam in a small target to produce hyperons
*Select particles produced in the forward direction.
*Collimate in the other directions. Interact as many of the other secondary particles as practical, especially the pions before they can decay to muons.

*Magnetically select the desired charge and momentum
*Do all of the above in as short a distance as possible to maximize the number of hyperons that survive. This puts a premium on

**high magnetic fields
**high resolution detectors
**high energy

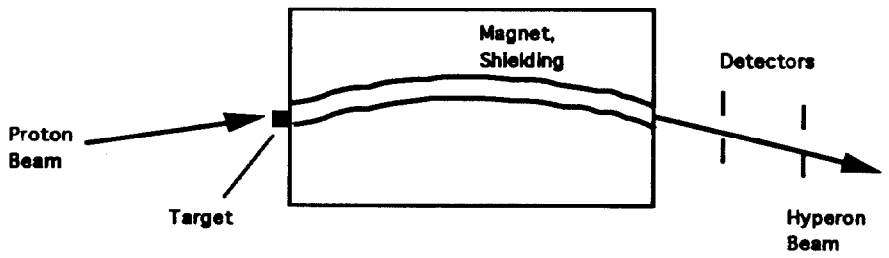

Figure 1. Essential Elements of a Charged Hyperon Beam (plan view)

In Figure 1, we see the essential elements of a generic hyperon beam. The Fermilab hyperon beam in Fermilab's Proton Center has a 7m long magnet, the hyperon magnet [8], with a vertical magnetic field of about 3.5 T. The inner portion of the magnet containing the channel is removable and can be fitted with a curved channel appropriate for a charged beam or a straight channel for a neutral beam. A set of magnets (not shown in Figure 1) upstream of the hyperon magnet allow for the angle of the proton beam impinging on the target to be varied either in the horizontal or vertical direction. This allows for the targeting angle to be varied between about $\approx\pm5$ mrad in either plane for 800 GeV incident protons. The transverse momentum, p_t, of the produced beam particle is just the product of the sine of the targeting angle and the hyperon momentum. Along with the Feynman x (x_F), it is used to characterize a hyperon beam. To a good approximation, x_F is just the ratio of the secondary particle momentum divided by the incident proton momentum. The ability to change the targeting angle in both the horizontal and vertical planes is important since it allows one to control the direction of the hyperon polarization.

Following the hyperon magnet is a set of high resolution spatial detectors. In the earlier beams these were spark chambers and then proportional chambers; now silicon strip detectors are used. In a recent configuration [2], a Cu target of 0.5 mm full width in the horizontal plane coupled with 50 μm pitch silicon strip detectors resulted in momentum resolution of $\approx$0.25% ($\Delta p/p$) and angular resolution of $\approx$10 μrad.

Early hyperon beams provided the first systematic measurements of hyperon fluxes and provided the "engineering" measurements needed for later beams. Figure 2 shows an early measurement [9] of these hyperon fluxes and a comparison with production of charged pions and kaons. This comparison is important since these are

the contaminants to the hyperon beam and their numbers will usually limit rates in the apparatus designed to study hyperon properties.

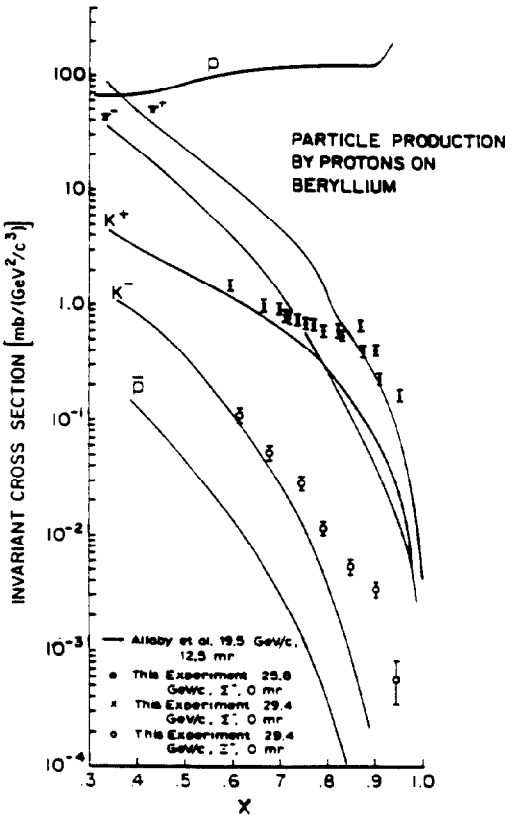

Figure 2. Hyperon Production Comparison Cross sections vs x_F

Figure 2 deserves some comments. Plotted is the measured production cross section as a function of x_F. These yields have been corrected for decay losses and extrapolated back to the production target. One notes a surprising fact: at large x_F the yield of Σ^- is greater than that of π^-, and that of Ξ^- is greater than that of K^-! This demonstrated that hyperons are produced copiously at high energies ($\approx$10% of all produced particles). It also showed the desirability of yet higher energy beams so that these high yields could be realized well downstream of the target. In Figure 3, I plot the hyperon decay lengths as a function of their momenta.

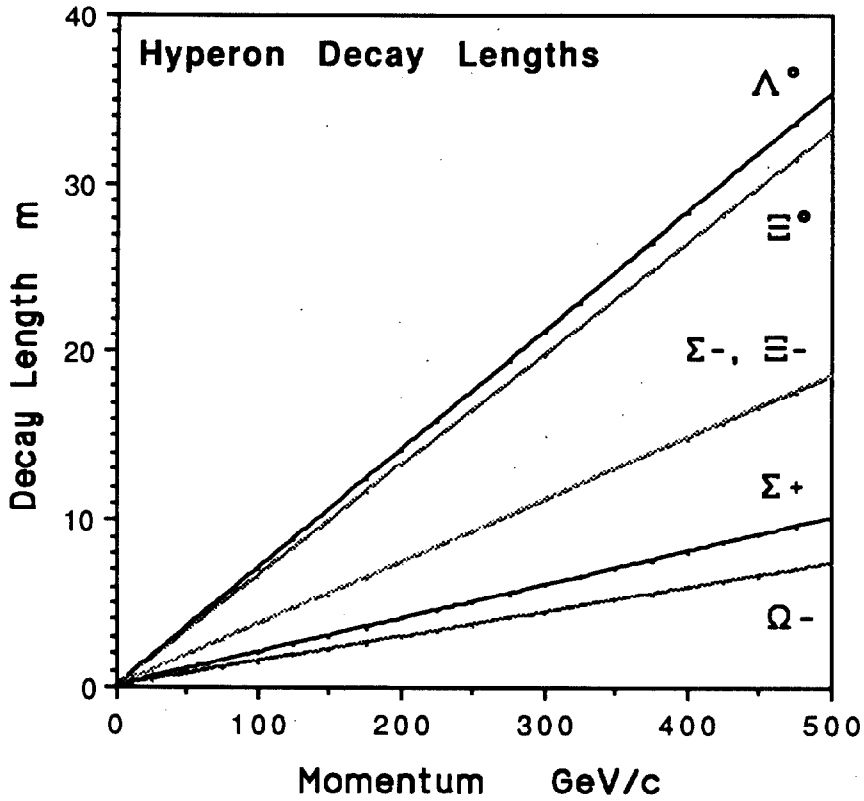

Figure 3. Hyperon decay lengths as a function of momentum

The hyperons of the baryon octet all have spin 1/2. Except for the Σ^0, which decays electromagnetically, all have their major decays modes mediated by the weak interactions. Because these weak decays do not conserve parity, information from the distribution of their decay products can be used to determine their spin direction. I illustrate this in Figure 4 where I schematically represent a polarized Σ^+ decaying to $\Sigma^+ \rightarrow p\pi^0$. The center of mass distribution of the decay pion in this decay can be written as

$$I(\cos\theta) \approx 1 + \alpha P \cos\theta$$

where P is the Σ^+ polarization and α is characteristic of the weak decay properties of the particle.

The physics of the decay is contained in α. If we just wish to measure a polarization or see the spin direction precess by a magnetic field we need not be concerned how nature gave us α; we can just use it. Note that we measure asymmetries, $A=\alpha P$, the product of α and P. The actual measurement can be the

number of protons which are emitted in direction of the +z axis ($N_\uparrow$) and those opposite to it ($N_\downarrow$). This gives us $A = 2(N_\uparrow - N_\downarrow)/(N_\uparrow + N_\downarrow)$.

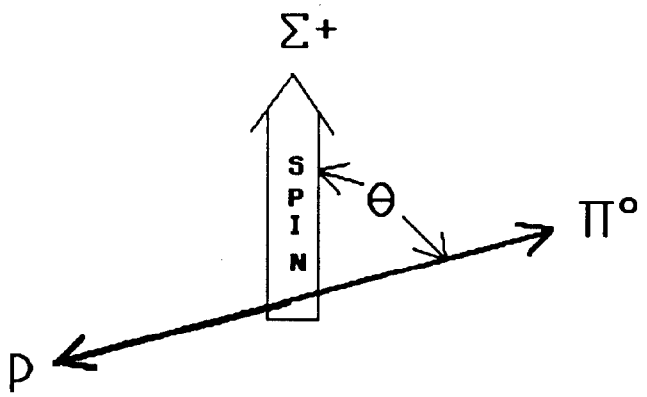

Figure 4. Decay of a polarized $\Sigma^+ \rightarrow p\pi^\circ$.

Note that we need to have both α and P non zero to measure a spin direction. Naturally, the larger the value of α, the easier it is to measure A and hence the polarization. Table 1 is a list [10] of some of the more important hyperon decay modes, branching ratios, and α parameters for these decays.

Table 1 Hyperon Decay Properties

Decay Mode	BR %	α
$\Sigma^+ \rightarrow p\pi^\circ$	51.6	-0.980±0.019
$\Sigma^+ \rightarrow n\pi^+$	48.3	0.068±0.013
$\Sigma^- \rightarrow n\pi^-$	99.8	-0.068±0.008
$\Sigma^- \rightarrow ne^-\bar{\upsilon}$	0.1	-0.519±0.104
$\Lambda^\circ \rightarrow p\pi^-$	64.1	0.642±0.013
$\Lambda^\circ \rightarrow n\pi^+$	35.7	0.65±0.05
$\Xi^\circ \rightarrow \Lambda^\circ\pi^\circ$	100.	-0.411±0.022
$\Xi^- \rightarrow \Lambda^\circ\pi^-$	100.	-0.456±0.014
$\Omega^- \rightarrow \Lambda^\circ K^-$	67.8	-0.026±0.026
$\Omega^- \rightarrow \Xi^\circ\pi^-$	23.7	0.09±0.14
$\Omega^- \rightarrow \Xi^-\pi^\circ$	8.6	0.05±0.21

From Table 1 we see that α for the various decay modes can assume a wide range of values. The decay $\Sigma^+ \rightarrow p\pi^\circ$ has α near its maximum negative value, making it easy to measure the Σ^+ polarization through this decay mode. The decay $\Sigma^- \rightarrow n\pi^-$ has a small (but non-zero) value of α making it necessary to have a large data sample and good control of systematic errors to get a measurement of its polarization.

In decays such as $\Xi^- \rightarrow \Lambda^\circ \pi^-$, where one also observes the subsequent decay, $\Lambda^\circ \rightarrow p\pi^-$, information about the spin direction of the Ξ^- is also contained in the decay distribution [5] of the decaying Λ°.

From Table 1, we see that for Ω^- decays, the values of α are all small and consistent with zero. In this case we must use the information from the subsequent Λ° decay to determine the parent polarization. Note that one can still measure the α parameters for the Ω^- decay even if the Ω^- is not polarized [7]. Although this is further complicated by the fact that the Ω^- has spin =3/2, similar procedures as for the Ξ^- decay have been developed [11].

Significant Λ° polarization was measured in the early Fermilab neutral hyperon beam [12]. Figure 5 shows data [13] for Λ° and $\overline{\Lambda}^\circ$ produced by 400 GeV protons. The polarization is plotted as a function of the transverse momentum, p_t, of the produced hyperon relative to the incident proton momentum. The Λ° polarization was found to be zero in the forward direction (as required by rotational symmetry for production from an unpolarized beam and target) and decreased linearly to $\approx$-20% at a transverse momentum (p_t) of $\approx$1.5 GeV/c. These early experiments also indicated that the polarization had little dependence on the initial energy of the proton or the target material. We use the conventional sign definition [14] for the inclusive hyperon polarization: a positive polarization is in the same direction as the cross product of the incident beam direction with the produced hyperon direction.

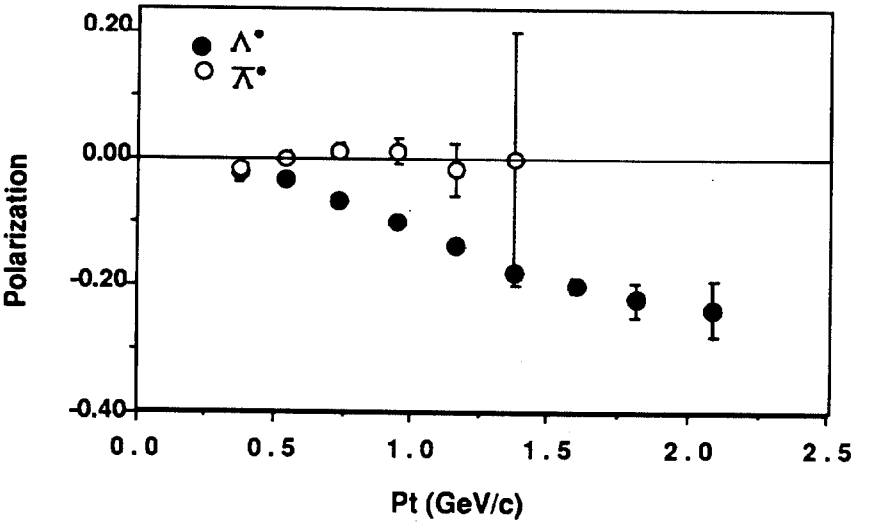

Figure 5. Polarizations of particle Λ° and $\overline{\Lambda}^\circ$

The clear evidence (Figure 5) that Λ° are produced with significant polarization came as a surprise. These polarizations have generally been attributed to peripheral mechanisms in which some of the proton valence quarks assimilate a strange quark from the sea to form a polarized hyperon.

The empirical conjecture that the more quarks incorporated from the sea reduces the produced hyperon polarization seemed to be confirmed by measurements of the polarization [11, 15-22], of $\Sigma^\pm$, Ξ^-, and Ω^- hyperons. Figure 6 shows the measured polarizations [23] of some other hyperons. Plotted here is the polarization as a function of the hyperon momentum at a fixed production angle. Since $p_t = P_h \sin\theta$, where P_h is the hyperon momentum and θ the production angle, the horizontal axis is proportional to p_t. These are all produced by 400 GeV protons. Significant polarizations seem to be a general property of hyperon production at high energies.

In these interactions, the Λ° is a leading particle and the $\overline{\Lambda}^\circ$ is not. Might this be significant? One sees each of the hyperons being produced with polarization of $\approx$10-20% at $p_t \approx 1$ GeV/c. The fact that early experiments had shown $\overline{\Lambda}^\circ$ to be unpolarized, where in the same kinematic range Λ° was polarized, lent credence to the idea that polarization is a leading particle effect. This was supported by measurements [11] showing the Ω^- to be unpolarized in this same kinematical region. Since the Ω^- is composed of three strange valence quarks it contains none of the valence quarks of the incident proton.

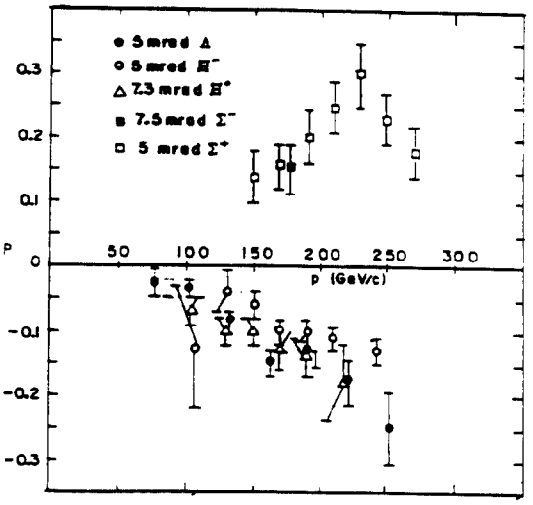

Figure 6. Polarization of other hyperons..
Plotted is the polarization vs hyperon momentum at fixed angles.
The horizontal axis is thus proportional p_t.

However, recent data have cast great doubt on this picture. Measurement of the $\overline{\Xi}^+$ polarization by the Fermilab E756 group [24], (Figure 7) shows $\overline{\Xi}^+$ to be polarized by about the same amount as the Ξ^-.

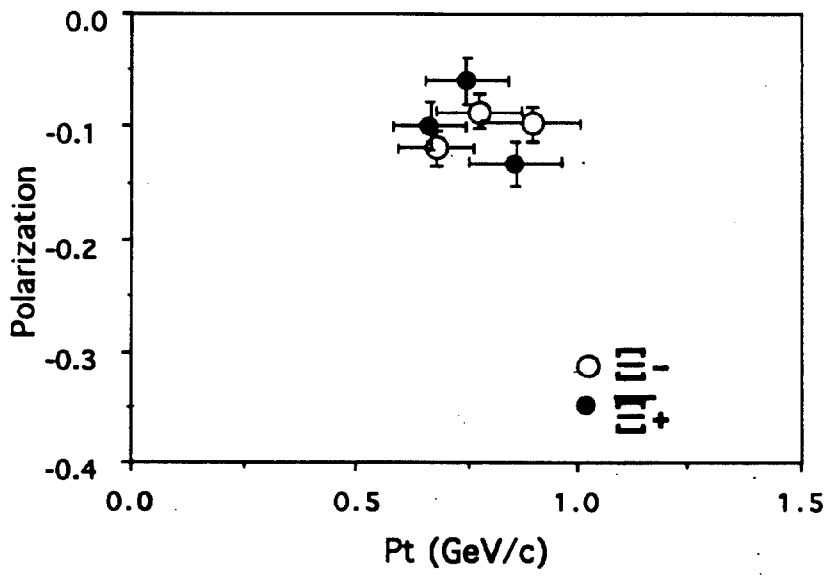

Figure 7 . Ξ^- and $\overline{\Xi}^+$ polarization

Let me illustrate the performance of recent Fermilab hyperon experiments by showing you results from our E761 group. I show this to illustrate the capabilities of modern hyperon beams in statistics and resolution. We have measured [25] the polarization of 375 GeV/c Σ^+ and $\overline{\Sigma}^-$ produced by 800 GeV protons on a Cu target. The Σ^+ was detected via its decay $\Sigma^+ \to p\pi^\circ$ and the $\overline{\Sigma}^-$ through its charge conjugate decay $\overline{\Sigma}^- \to \overline{p}\,\pi^\circ$.

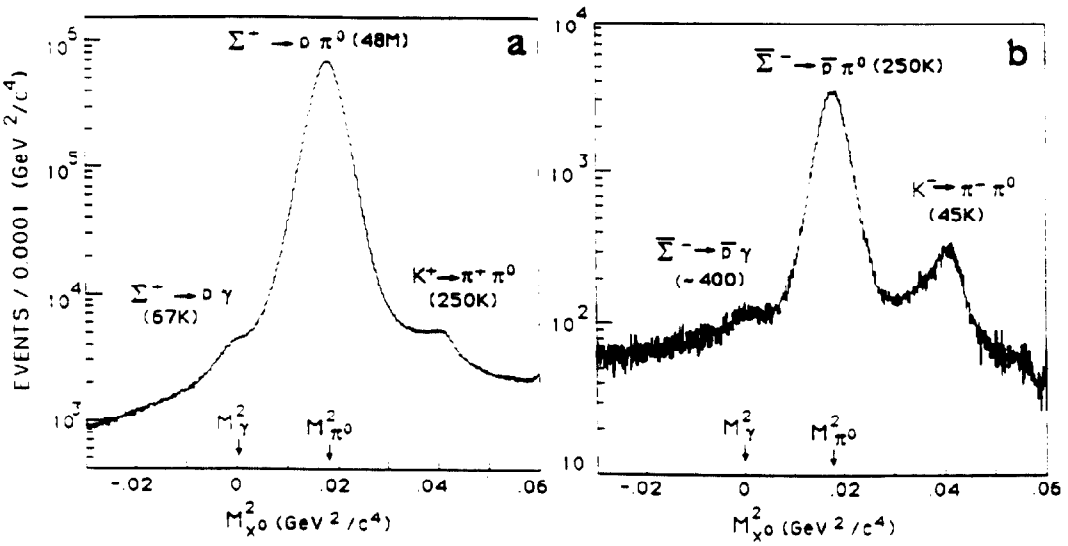

Figure 8. Event distributions of the mass squared of the missing neutral particle (X°) for the hypothesis $\Sigma^+ \to pX^\circ$ for positive and negative beam candidates

Figure 8ab shows the reconstructed π^0 mass squared for the negative and positive beam. In the positive data one clearly observes the rare radiative decay, $\Sigma^+ \to p\gamma$, whose study was the major goal [2] of this experiment. Both this decay and the charge kaon decays are clearly visible but can be easily removed by making a selection on the missing mass.

Figure 9 shows the measured polarizations of Σ^+ and $\overline{\Sigma}^-$ as a function of p_t. In this data one sees that $\overline{\Sigma}^-$ are also produced with $\approx 8\%$ polarization near $p_t \approx 1$ GeV/c.

This Σ^+ data shows that the polarization increases with p_t, goes through a maximum near $p_t = 1$ GeV/c and then decreases. This is the first time this decrease has been observed in a high energy hyperon polarization.

The data of Figure 9 show points taken with both horizontal and vertical targeting for Σ^+ and $\overline{\Sigma}^-$. In horizontal targeting, the incident beam direction is changed in the horizontal (H) plane producing polarization in the same plane (vertical) as the magnetic field of the hyperon magnet Thus there is no spin rotation as the hyperons traverse the magnet. Targeting in the vertical (V) plane produces a polarization in the horizontal plane, perpendicular to the magnet field, thus producing maximum spin rotation as would be desired for measurement of a magnetic moment.

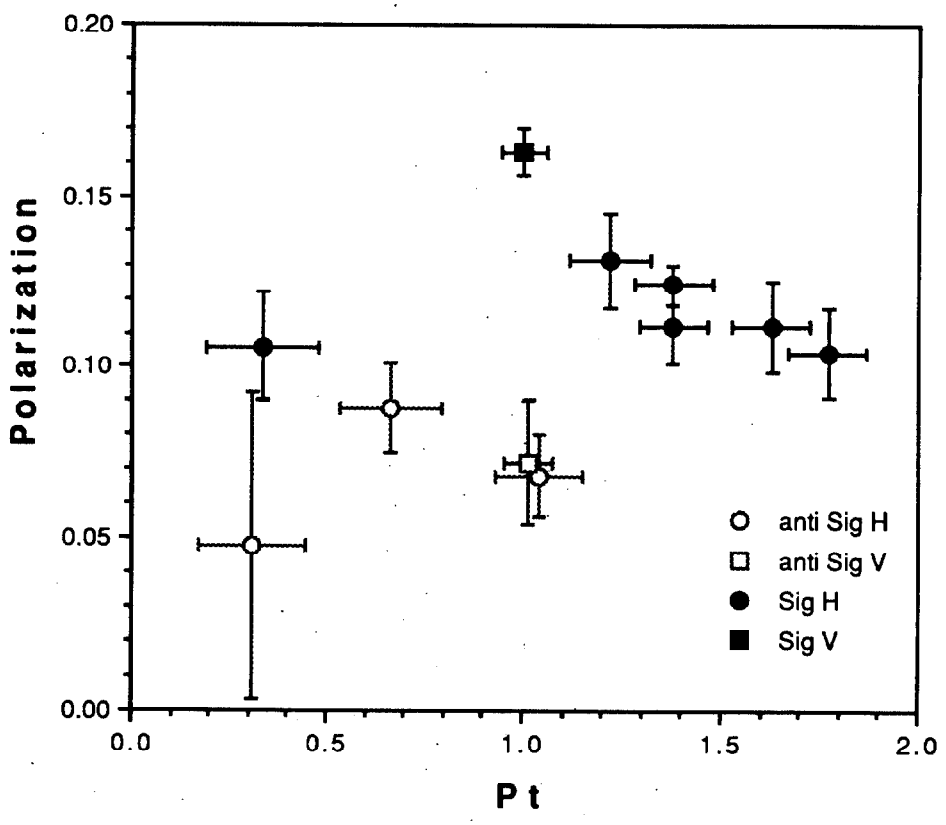

Figure 9. Σ^+ and $\overline{\Sigma}^-$ polarization as a function of Pt

This experiment demonstrated that $\bar{\Sigma}^-$ hyperons are produced in high energy collisions with polarization of the same sign though of smaller magnitude than that of Σ^+. This observation is similar to the recent Fermilab results [24] which showed that both Ξ^- and $\bar{\Xi}^+$ are polarized with about the same magnitude. This would indicate that the polarization of antihyperons is a common phenomenon, and we should now turn our attention to why the $\bar{\Lambda}^\circ$ are not produced polarized.

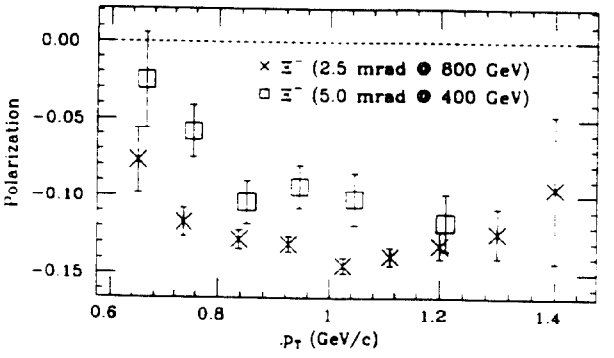

Figure 10 Comparison of Ξ^- polarization at 400 and 800 GeV.

The early data indicated that there was no strong energy dependence to hyperon polarization. However, recent high statistics data comparing hyperon production at 400 and 800 GeV indicate a much more complex phenomena. Figure 10 shows data from Fermilab E756 comparing Ξ^- production at 400 and 800 GeV [20, 26]. The 400 GeV protons used a 5 mrad production angle whereas the 800 GeV experiment was a 2.5 mrad. Thus the data was matched in both x_F and pt. One sees that the magnitude of the polarization increases with the incident proton energy.

Figure 11 show the polarization as a function of p_t for Σ^+ at 400 GeV from Fermilab experiments E497 [15] and E620 [16] and compares them with E761 [27] at 800 GeV. Note that the E620 data is from production on a Be target. The others use a Cu target. However, at least for Λ° production, the nature of the target material does not seem to have a major effect on hyperon polarization. Pondrom [5] has a good summary of target material dependence of hyperon production and polarization data. All of the Σ^+ data are in a range $0.47 < x_F < 0.53$. This data also shows a clear energy dependence of the Σ^+ polarization. Here, in contrast to the Ξ^- data of Figure 9, the polarization decreases in the same energy range.

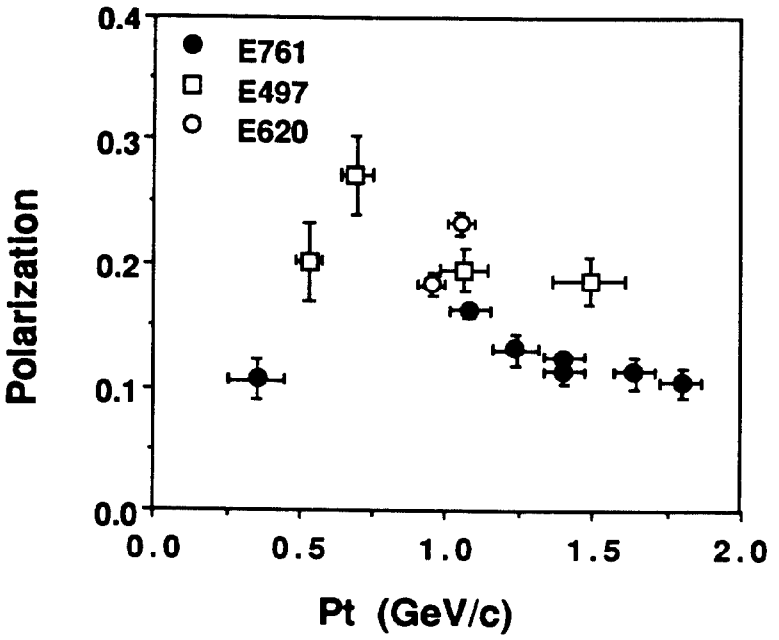

Figure 11. Comparison of Σ^+ polarization at 400 (open points) and 800 GeV (black points).

Fermilab E799, in a very recent preliminary result [28], using the Λ° contamination in their K° beam has measured the Λ° polarization at 800 GeV. This measurement and the comparison with a previous measurements [29] at 400 GeV is shown in Figure 12. This very nice comparison shows no energy dependence of the polarization!

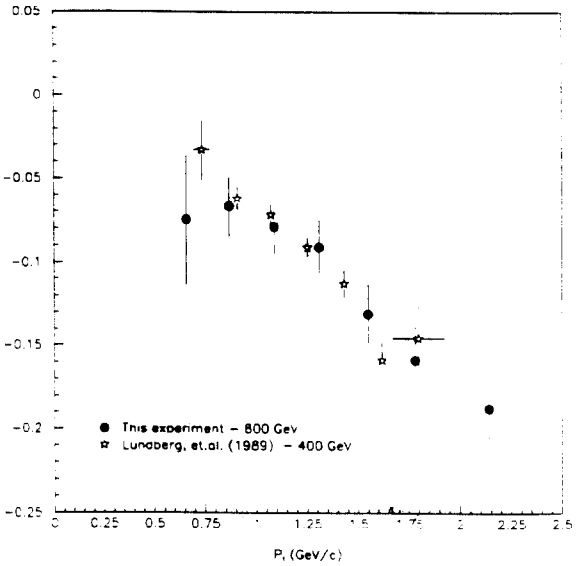

Figure 12 Comparison of Λ° polarization at 400 and 800 GeV.

We now have good comparisons of the Σ^+, Ξ^-, and Λ° polarizations at 400 and 800 GeV and find the astonishing result that the first decreases, the second increases, and the last remains constant with energy.

Among the many proposed models for hyperon (but not antihyperon) polarization [30-33], let me mention two approaches to the polarization question - both involving similar leading particle effects. One is that of the Lund group [34] whose model assumes $q\bar{q}$ pairs are produced from the sea via the breaking of a QCD string but conserving local angular momentum. DeGrand and Miettinen [35] propose two simple rules: quarks which gain longitudinal momentum combine with spins down; quarks which lose longitudinal momentum combine with spins up. This is equivalent to a Thomas precession and a spin orbit coupling. Both models explain much of the hyperon data. The magnitudes of some of the polarizations are at odds with each of the models. Other models are discussed in a review by P. Kroll [36] and is recommended although it was done before the polarizations of the $\bar{\Xi}^+$ and $\bar{\Sigma}^-$ were known. A recent model using a Regge pole approach [37] gives qualitatively good agreement with Σ^+ polarization data. None of the above models address the polarizations of the antihyperons or the above mentioned hyperon polarization energy dependence.

The only publication [38] that I am aware of that offers an explanation for hyperon (and antihyperon) polarization does so in the framework an optical potential model. In this model the polarization occurs at the surface of the nucleon and the process applies naturally to both hyperons and antihyperons. The last couple of years have seen a major addition to the available data on the polarization of both hyperons and antihyperons.

Clearly the $\Lambda^\circ/\bar{\Lambda}^\circ$, $\Xi^-/\bar{\Xi}^+$, and $\Sigma^+/\bar{\Sigma}^-$ systems exhibit a rich and challenging set of polarization phenomena that cry out for insightful ideas.

The phenomenon of crystal channeling [39, 40] has been of interest because of the very high effective magnetic fields that are involved. Figure 13 illustrates this phenomenon. Figure 13 depicts a crystal oriented so that a charged beam enters almost parallel to the crystal axis. A positively charged particle entering thus finds itself in a potential well formed by the positively charged arrays of nuclei. It is trapped -channeled- in this potential if the incident angle is near the crystal plane. If the angle is too large it passes through the crystal without being channeled as indicated in the same figure.

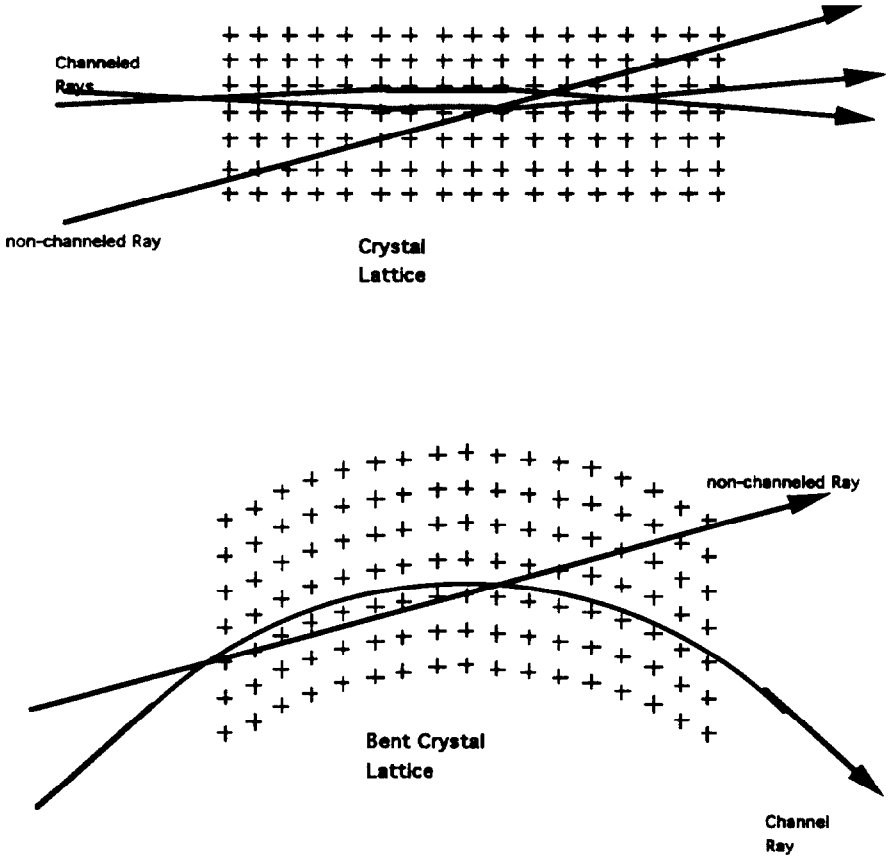

Figure 13ab. Channeling in straight and bent crystal

If one now bends the crystal as depicted in Figure 13b, one finds that one also bends the channeled beam [39]. From the momentum of the particle and the bend angle one realizes that the effective magnetic fields inside the crystal can be very large. Can these same large fields be used to precess the spin direction of a polarized beam? Fermilab E761 attempted to see this effect in a subsidiary experiment [41]. A beam containing Σ^+ hyperons is a good candidate for investigating this effect since they can be produced polarized and have a large decay asymmetry parameter (α= -0.98) for the common decay mode, $\Sigma^+ \rightarrow p\pi^\circ$. Hence, one can readily measure their spin direction from the decay distribution.

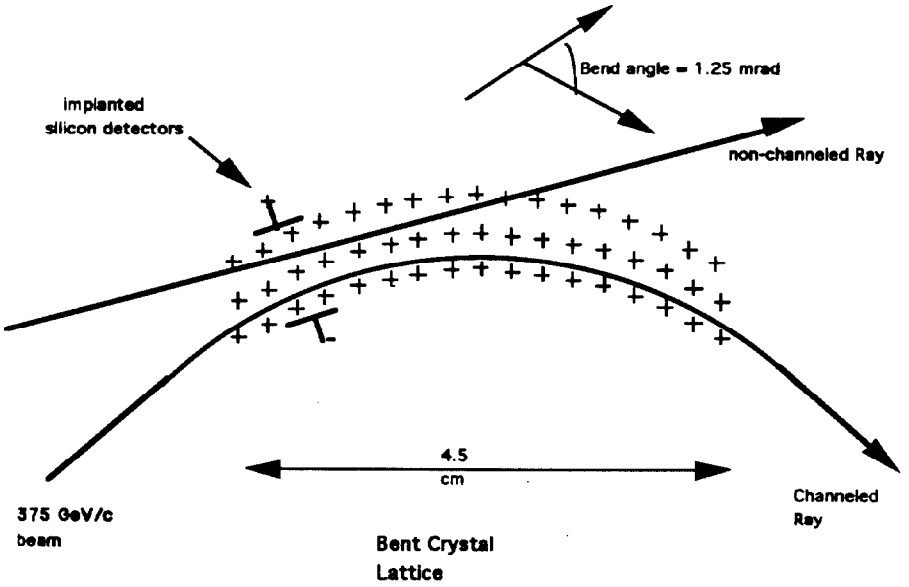

Figure 14 E761 crystal setup for channeling

Figure 14 schematically shows the crystal configuration used in E761. A single crystal of silicon was placed in a 375 GeV/c beam which contained about 1% Σ^+ (the rest being mainly protons and π^+). This crystal was also implanted with solid state energy loss detectors so that the energy deposited in the crystal could be measured for each incident particle. Apparatus upstream (not shown) of the crystal measured the incident particle momentum and angle (with a precision of $\approx$0.2% and $\approx$ 10μrad respectively). A downstream spectrometer (also not shown) measured the particle momentum and trajectory a second time. Figure 15 shows some results [41] where no distinction is made between particle types. Thus it contains mostly protons and π^+. Figure 15a shows the difference between the angle measured entering and exiting the crystal. One sees a peak at about 1.65 mrad which is the known bending angle of the crystal.

Another characteristic is that the channeled particles lose less energy due to ionization than their non-channeled counterparts. Figure 15b shows the energy deposition in the crystal for those events which triggered the apparatus The peak at lower energy loss values is due to channeled particles. The solid line through the non channeled portion is a theoretical Landau distribution.

In this experiment the spin precession of channeled particles in bent crystals has been observed [41] for the first time. These crystals provided an effective magnetic field of 45 T which resulted in a measured spin precession of 60±17°. This agrees with the prediction of 62±2° using the world average [10] of Σ^+ magnetic moment measurements. This new technique gives a Σ^+ magnetic moment of 2.40±0.46±0.40 μ_N where the quoted uncertainties are statistical and systematic respectively. No evidence of depolarization in the channeling process.

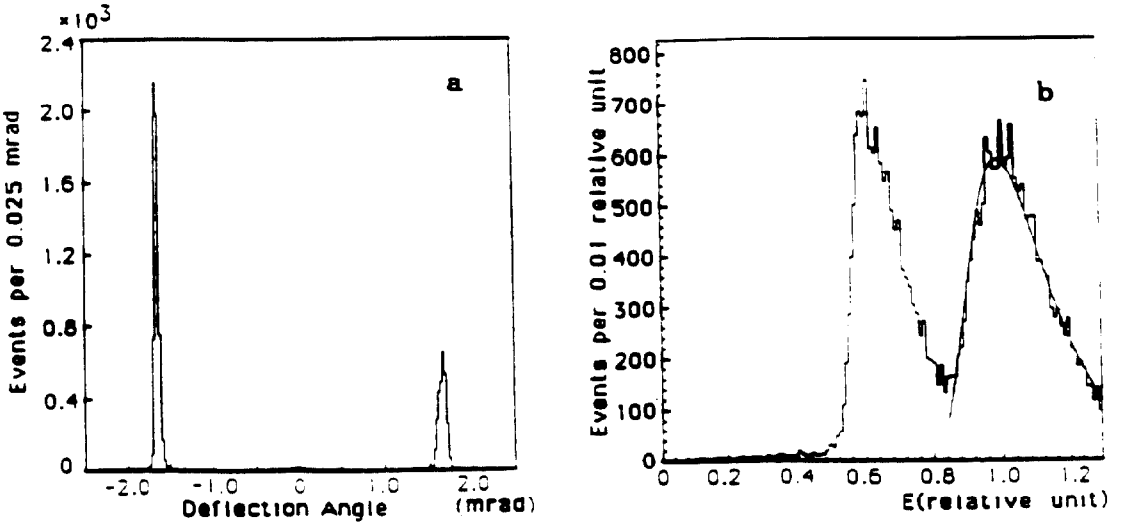

Figure 15 Crystal Channeling Data.
(a) Deflection of beam by crystal.
(b) Energy loss for non-channeled particles.

The crystal bend angle of 1.65 mrad was chosen to match the acceptance of the downstream spectrometer. The crystal was bent to angles as large as 10 mrad (without breaking!) which would correspond to an effective magnetic field of ≈275. T!

Figure 16 shows the history of Σ^+ magnetic moment [15, 16, 42-47] measurements. Note that in the early 1970's this would have been the most precise measurement of the Σ^+ magnetic moment.

An exciting possibility is the application of this technique to charmed baryons which have a much shorter lifetimes [10] than Σ^+. Note that at 500 GeV/c the Λ^+_c and Ξ^+_c would have decay lengths of 1.2 and 2.6 cm respectively.

The phenomena of hyperon polarization in high energy interactions has forced us to rethink the basic physics of the production of polarized particles in the strong interactions.

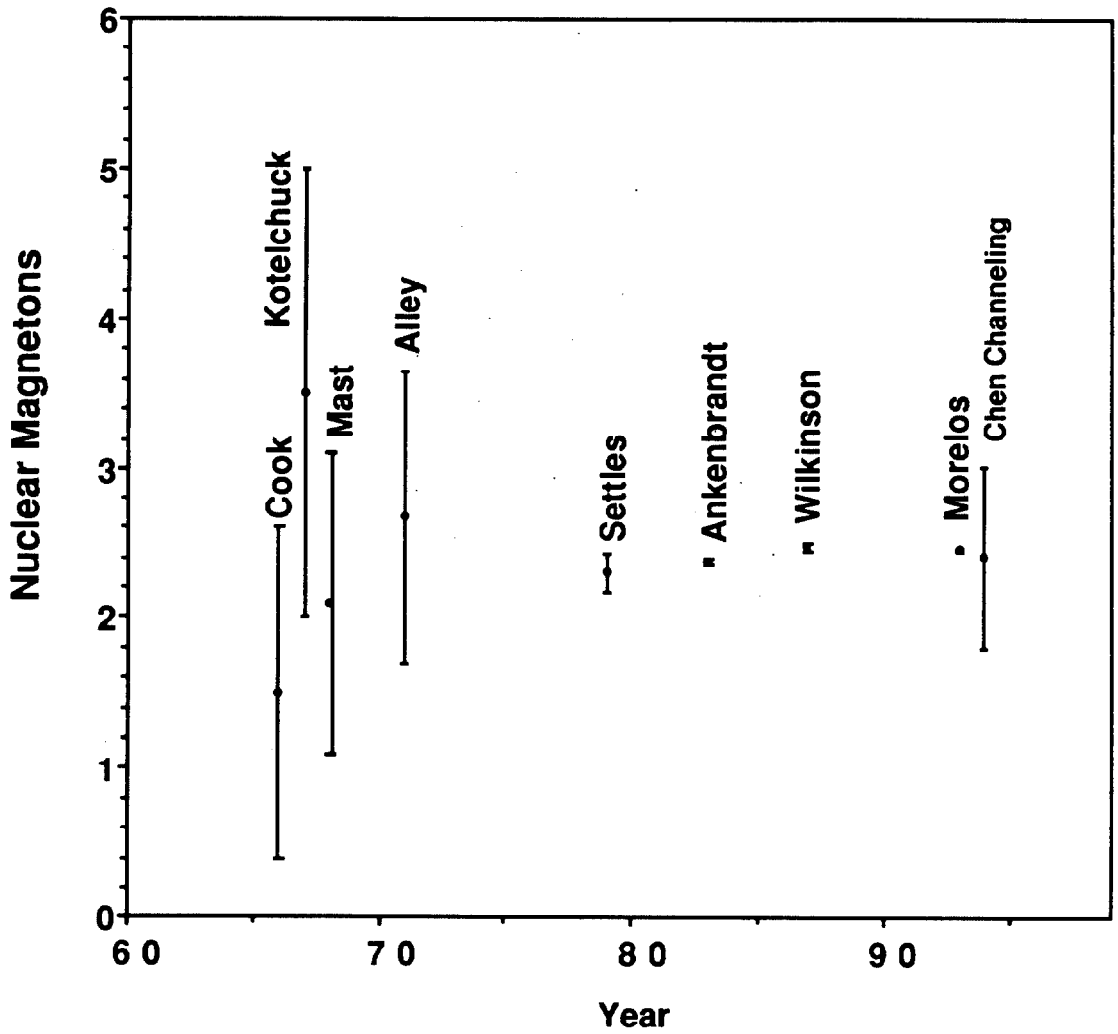

Figure 16 History of Σ^+ Magnetic Moment Measurements

Future Prospects.

I have tried to give a broad description of the development of hyperon beams and some of the physics they have done. The direction for future devolopments follows the lead of the CERN SPS hyperon experiment (CERN WA62). We have only been discussing states composed of the three lowest mass quarks. From Figure 17, it is clear that there is a much richer structure when the c (charm) quark is also included.

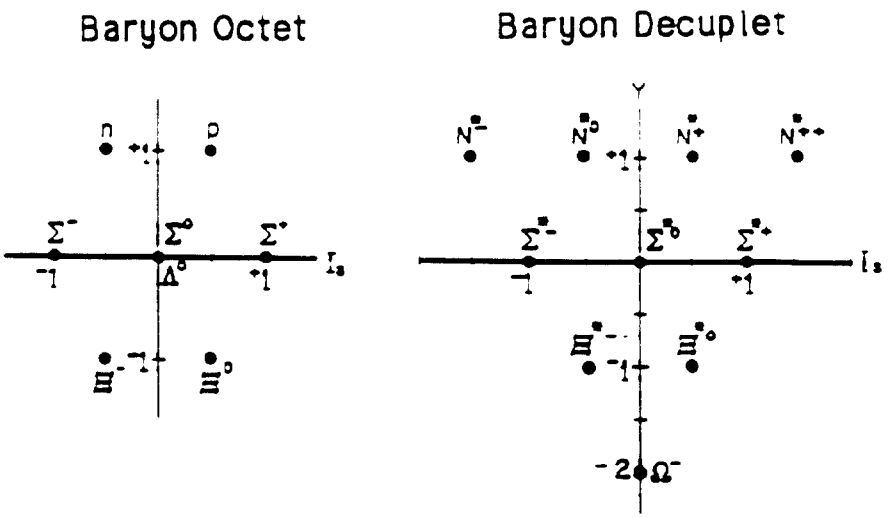

Figure 17. Three quark states of $1/2^+$ and $3/2^+$ which form the SU(4) equivalents to the baryon octet and nonet states.

The study of charm states in hadronic interactions has been driven by the development of new detector technologies and has proceeded in three phases. The first phase came shortly after the initial discovery of charm. Many planned experiments modified their apparatus in an attempt to see these states. Most of these were failures. The notable exceptions was CERN WA62 which discovered the A^+ [48], a csu state, and the T° [49], a css state, using a beam of Σ^- hyperons. In the modern nomenclaure of Figure 17 these are Ξ_c^{*+} and $\Omega^{*\circ}_c$ states respectively.

The second phase came with the development of silicon strip detectors which provided the additional resolution to clearly identify the detached vertex of charm decays. These experiments (many of whose successors are still taking data) were able to map out the charm spectrum, measure branching rates, lifetimes, etc. CERN experiment WA89 (the successor to WA62) is just now reporting on its exciting new data [50].

The third phase is exemplified by Femilab E781 which will use a higher energy and more intense Σ^- beam than WA89. This experiment will be able to trigger on detached vertices using a powerful array of computers ($\approx$1000 MIPS). This experiment will take data in the next Fermilab fixed target run.

It is clear that a rich program of charmed baryon spectroscopy is before us. It is one in which an incident projectile carrying a strange quark has an advantage in producing states with both charm (or perhaps even beauty) and strangeness. Fermilab E781 which will run in the next Fermilab fixed target run should make a very significant contribution to this program.

I would like to acknowledge many important discussions with my Fermilab hyperon colleagues. This work is supported by the U.S. Department of Energy under contract DE-AC02-76CH03000.

References

1. S.Y. Hsueh *et al.*, Phys. Rev. Lett **54**, 2399 (1985).
2. M. Foucher *et al.*, Phys. Rev. Lett. **68**, 3004 (1992).
3. P. Cooper, this meeting, 1993
4. J. Lach and L. Pondrom, Annu. Rev. Nucl. Part. Sci. **29**, 203 (1979).
5. L. Pondrom, Phys. Rep. **122**, 57 (1985).
6. J.M. Gaillard and G. Savage, Ann. Rev. Nucl. Part. Sci. **34**, 351 (1984).
7. M. Bourquin and J.P. Repellin, Phys. Reports **114**, 100 (1984).
8. T.R. Cardello *et al.*, Phys. Rev. **32**, 1 (1985).
9. V. Hungerbuhler *et al.*, Phys. Rev. **D12**, 1203 (1975).
10. Particle Data Group, Phys. Rev. **D45**, 1 (1992).
11. K.B. Luk *et al.*, Phys. Rev **D38**, 19 (1988).
12. G. Bunce *et al.*, Phys. Rev. Lett. **36**, 1113 (1976).
13. K. Heller *et al.*, Phys. Rev. Lett. **41**, 607 (1978).
14. Basel Convention, Helv. Phys. Acta Suppl. VI, (1961).
15. C. Ankenbrandt *et al.*, Phys. Rev. Lett. **51**, 863 (1983).
16. C. Wilkinson *et al.*, Phys. Rev. Lett. **58**, 855 (1987).
17. Y.W. Wah *et al.*, Phys. Rev. Lett. **55**, 2551 (1985).
18. L. Deck *et al.*, Phys. Rev. **D28**, 1 (1983).
19. G. Zapalac *et al.*, Phys. Rev. Lett **57**, 1526 (1986).
20. R. Rameika *et al.*, Phys. Rev. **D33**, 3172 (1986).
21. L.H. Trost *et al.*, Phys. Rev. **D40**, 1703 (1989).
22. H.T. Diehl *et al.*, Phys. Rev. Lett. **67**, 804 (1991).
23. K. Heller, Proceedings of the 9th International Symposium on High Energy Spin, Bonn, Germany, p 97, Springer-Verlag (1990).
24. P.M. Ho *et al.*, Phys. Rev. Lett. **65**, 1713 (1990).
25. A. Morelos *et al.*, Phys. ReV. Lett. **71**, 2172 (1993).
26. J. Duryea *et al.*, Phys. Rev. Lett. **67**, 1193 (1991).
27. A. Morelos, Ph.D. Thesis, Centro de Investigacion y de Estudios Avanzados del IPN, Mexico ,1992 (unpublished).
28. E. Ramberg, E799, personal communication, 1993
29. B. Lundberg *et al.*, Phys. Rev. **D40**, 3557 (1989).
30. J. Szwed Phys. Lett. **105B**, 403 (1981).
31. P. Cea *et al.*, Phys. Lett. **209B**, 333 (1988).
32. J. Soffer and N.A. Tornqvist Phys. Rev. Lett. **68**, 907 (1992).
33. W.G.D. Dharmaratna and G.R. Goldstein Phys. Rev. **41**, 1731 (1990).
34. B. Andersson *et al.*, Phys. Lett. **85B**, 417 (1979).
35. T.A. DeGrand and H.I. Miettinen Phys. Rev. **24**, 2419 (1981).
36. P. Kroll, High Energy Spin Physics, Minneapolis, Minnesota, p 48, American Institute of Physics Conference Proceedings No. 187 (1988).
37. R. Barni *et al.*, Phys. Lett. **B296**, 251 (1992).

38. Y. Hama and T. Kodama, Phys. Rev. **D40**, 3116 (1993).
39. J.S. Forster *et al.*, Nucl. Phys. **B318**, 301 (1989).
40. R. Carrigan and J.A. Ellison, Relativistic Channeling (Plenun Press, New York, 1987).
41. D. Chen *et al.*, Phys. Rev. Lett. **69**, 3286 (1992).
42. V. Cook *et al.*, Phys. Rev. Lett. **17**, 223 (1966).
43. D. Kotelchuck *et al.*, Phys. Rev. Lett. **25**, 1166 (1967).
44. T.S. Mast *et al.*, Phys. Rev. Lett. **23**, 1312 (1968).
45. P.W. Alley *et al.*, Phys. Rev. **D3**, 75 (1971).
46. R. Settles *et al.*, Phys. Rev. **D20**, 2154 (1979).
47. A. Morelos *et al.*, Phys. Rev. Lett. **71**, 3417 (1993).
48. S.F. Biagi *et al.*, Phys. Lett. **122B**, 455 (1983).
49. S.F. Biagi *et al.*, Z. Phys. **C28**, 175 (1985).
50. B. Povh, this meeting, 1993